Thermodynamic Evidence of Proximity to a Kitaev Spin Liquid in $Ag_3LiIr_2O_6$

Faranak Bahrami,[1] William Lafargue-Dit-Hauret,[2,3] Oleg I. Lebedev,[4] Roman Movshovich,[5] Hung-Yu Yang,[1] David Broido,[1] Xavier Rocquefelte,[2] and Fazel Tafti[1,*]

[1]*Department of Physics, Boston College, Chestnut Hill, Massachusetts 02467, USA*
[2]*Univ Rennes, CNRS, ISCR (Institut des Sciences Chimiques de Rennes) UMR 6226, F-35000 Rennes, France*
[3]*Physique Théorique des Matériaux, CESAM, Université de Liège, B-4000 Sart Tilman, Belgium*
[4]*Laboratoire CRISMAT, ENSICAEN-CNRS UMR6508, 14050 Caen, France*
[5]*MPA-CMMS, Los Alamos National Laboratory, Los Alamos, New Mexico 87545, USA*

(Received 27 May 2019; revised manuscript received 4 September 2019; published 3 December 2019)

Kitaev magnets are materials with bond-dependent Ising interactions between localized spins on a honeycomb lattice. Such interactions could lead to a quantum spin-liquid (QSL) ground state at zero temperature. Recent theoretical studies suggest two potential signatures of a QSL at finite temperatures, namely, a scaling behavior of thermodynamic quantities in the presence of quenched disorder, and a two-step release of the magnetic entropy. Here, we present both signatures in $Ag_3LiIr_2O_6$ which is synthesized from α-Li_2IrO_3 by replacing the interlayer Li atoms with Ag atoms. In addition, the dc susceptibility data confirm the absence of a long-range order, and the ac susceptibility data rule out a spin-glass transition. These observations suggest a closer proximity to the QSL in $Ag_3LiIr_2O_6$ compared to its parent compound α-Li_2IrO_3 that orders at 15 K. We discuss an enhanced spin-orbit coupling due to a mixing between silver d and oxygen p orbitals as a potential underlying mechanism.

DOI: 10.1103/PhysRevLett.123.237203

An exciting frontier in condensed matter physics is to design materials where the spin degrees of freedom avoid a magnetically ordered ground state despite strong exchange interactions. Such compounds release the spin entropy by forming a quantum entangled ground state known as the quantum spin liquid (QSL) [1–4]. Among various proposals for a QSL, the Kitaev model is especially appealing because it is exactly solvable and can be engineered in real materials [5,6]. The model consists of bond-dependent Ising interactions between localized $S = 1/2$ spins on a honeycomb lattice, $\mathcal{H}_K = -\sum K_\gamma \mathbf{S_i}^\gamma \mathbf{S_j}^\gamma$ [1,5]. The ground state is analytically solved by fractionalizing the spin-1/2 operators ($\mathbf{S_i}$) into itinerant and localized Majorana fermions [5,7]. Recent Monte Carlo (MC) simulations suggest that by decreasing temperature, the two types of Majorana fermions undergo two successive crossovers [8,9]. First, at a higher temperature T_H, the itinerant Majorana fermions form coherent bands. Second, at a lower temperature T_L, the localized Majorana fermions form Z_2 gauge fluxes aligned on all hexagons. Evidence of such behavior is reported in layered iridium oxides, α-Li_2IrO_3 and Na_2IrO_3, with a honeycomb network of edge-sharing IrO_6 octahedra [Fig. 1(a)] where Ir^{4+} assumes a $J_{\text{eff}} = 1/2$ state due to strong spin-orbit coupling (SOC) [10]. However, both compounds exhibit long-range antiferromagnetic (AFM) ordering and fail to reach a QSL ground state [11–13]. Thus, a complete model Hamiltonian for the honeycomb iridates must include non-Kitaev interactions:

$$\mathcal{H} = \sum_{\langle i,j\rangle \in \alpha\beta(\gamma)} [-K_\gamma S_i^\gamma S_j^\gamma + J\mathbf{S}_i \cdot \mathbf{S}_j + \Gamma(S_i^\alpha S_j^\beta + S_i^\beta S_j^\alpha)], \quad (1)$$

where the Kitaev term (K) favors QSL, the Heisenberg term (J) favors AFM order, and the off-diagonal exchange term (Γ) controls details of the magnetic order [6,14]. Both α-Li_2IrO_3 and Na_2IrO_3 seem to be closer to the Heisenberg limit ($J > K$) despite evidence of a strong Kitaev interaction [15,16].

Recently, two approaches have been taken to bring the candidate materials closer to the Kitaev limit. The first approach was to bring the Ir-O-Ir bond angles closer to 90° and maximize a destructive quantum interference between the Heisenberg interactions across each pair of superexchange paths [6] [Fig. 1(b)]. This idea led to the discovery of α-$RuCl_3$ [18], where the AFM order occurs at $T_N = 7$ K [19] smaller than $T_N = 15$ K in iridates. The second approach was to induce a random bond disorder within the honeycomb layers which is achieved in $H_3LiIr_2O_6$ due to hydrogen intercalation and a heavy stacking disorder [20–22]. Here, we present a third approach based on modifying the interlayer bonds. We replace the Li atoms between the layers of α-Li_2IrO_3 [Fig. 1(c)] with Ag atoms to produce $Ag_3LiIr_2O_6$ [Fig. 1(d)]. The honeycomb layers of $Ag_3LiIr_2O_6$ are identical to those of its parent compound but the chemical bonds between the layers are modified. The interlayer Li atoms in α-Li_2IrO_3 are octahedrally coordinated with six oxygens, three on top and three at the bottom, whereas the Ag atoms in $Ag_3LiIr_2O_6$ are linearly

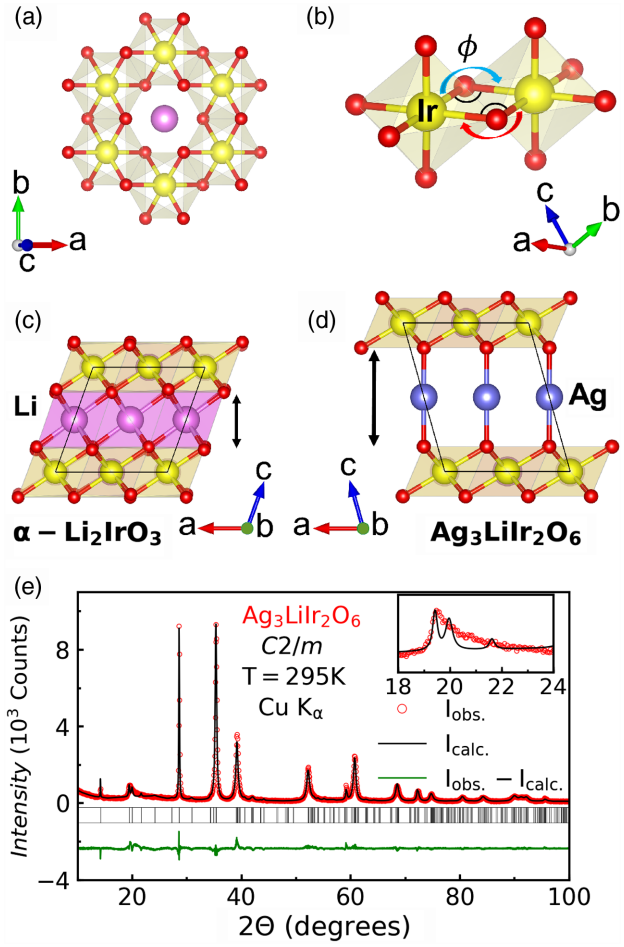

FIG. 1. (a) Honeycomb lattice of edge-sharing IrO_6 octahedra in both α-Li_2IrO_3 and $Ag_3LiIr_2O_6$. (b) Heisenberg exchange paths between neighboring octahedra. (c) Octahedral coordination of Li atoms between the layers of α-Li_2IrO_3. (d) Linear (dumbbell) coordination of Ag atoms between the layers of $Ag_3LiIr_2O_6$ which leads to increasing the interlayer separation. (e) Rietveld analysis with a magnified view of the Warren line shape due to stacking faults (See also Figs. S1 and S3 [17]).

coordinated with two oxygens [Figs. 1(c), 1(d)]. The weaker O-Ag-O dumbbell bonds result in a 30% increase of the interlayer separation. Our experiments reveal three thermodynamic signatures that suggest $Ag_3LiIr_2O_6$ is closer to the Kitaev limit than its parent compound α-Li_2IrO_3. First, the AFM peak in the magnetic susceptibility of α-Li_2IrO_3 at 15 K is absent in $Ag_3LiIr_2O_6$. Second, a scaling behavior is observed in the ac susceptibility over three decades of T/H consistent with a random singlet scenario in QSL candidates [23]. Third, a two-step release of the magnetic entropy at $T_H = 75$ and $T_L = 13$ K is observed consistent with recent MC simulations [8,9].

Polycrystalline samples of $Ag_3LiIr_2O_6$ were prepared via a topotactic reaction at 350 °C for 24 h according to

$$2Li_2IrO_3 + 3AgNO_3 \rightarrow Ag_3LiIr_2O_6 + 3LiNO_3. \quad (2)$$

The precursor α-Li_2IrO_3 was synthesized following prior reports [10]. We also synthesized the nonmagnetic $Ag_3LiSn_2O_6$ using a similar procedure, and used it as a phonon analogue of $Ag_3LiIr_2O_6$ in the heat capacity analysis. Powder x-ray diffraction (PXRD) was performed using a Bruker D8 ECO instrument. A combination of the FullProf suite and Vesta software was used for the Rietveld refinement and crystal visualization [24,25]. Magnetization and heat capacity were measured using Quantum Design MPMS3 and PPMS Dynacool, respectively.

Structure.—Figure 1(e) shows the PXRD pattern of $Ag_3LiIr_2O_6$ with a Rietveld refinement in the same space group ($C2/m$) as its parent compound α-Li_2IrO_3 [17,26]. Although a prior work has suggested the space group $R\bar{3}m$ [27], a recent structural analysis of the material agrees with our solution [28]. The asymmetric broadening (Warren line shape) of the peaks between 18° and 24° in the inset of Fig. 1(e) is commonly observed in the layered honeycomb structures [29–31]. It is analyzed in Fig. S1 of the Supplemental Material and gives at least 5% of stacking disorder [17,32]. Our Rietveld refinement shows relatively small Debye-Waller factors for the Ag atoms [17] corresponding to well-defined Ag-O bonds unlike the H-O bonds in $H_3LiIr_2O_6$, where the region of stacking faults must be excluded to obtain a reasonable refinement [20]. Thus, the in-plane bond randomness in $H_3LiIr_2O_6$ [22] is negligible in $Ag_3LiIr_2O_6$. To gain further confidence on the reported oxygen positions and Ir-O-Ir bond angles, we subjected the crystallographic unit cell to a geometric optimization in the VASP code [17,33–35]. The results in Table I (and Fig. S2 of the Supplemental Material [17]) show an excellent agreement between the experimental and theoretical bond distances and angles. We performed the same analysis on α-Li_2IrO_3 and found comparable Ir-O-Ir bond angles between the two compounds (Table I). Thus, the cancellation between opposite Heisenberg exchange paths in Fig. 1(b) must be comparable between $Ag_3LiIr_2O_6$

TABLE I. Experimental and theoretical values of bond lengths and angles in $Ag_3LiIr_2O_6$ and α-Li_2IrO_3.

$Ag_3LiIr_2O_6$		
	Experimental	Theoretical
Ir1-O1-Ir1	96.5(3)°	97.54(0)°
Ir1-O2-Ir1	96.9(6)°	97.66(0)°
Ir1-O1	2.043(9) Å	1.988(0)°
Ir1-O2	2.046(5) Å	1.990(0)°
α-Li_2IrO_3		
	Experimental	Theoretical
Ir1-O1-Ir1	94.7(5)°	94.42(0)°
Ir1-O2-Ir1	95.3(8)°	94.56(0)°
Ir1-O1	2.015(13) Å	2.003(0)°
Ir1-O2	2.080(19) Å	2.010(0)°

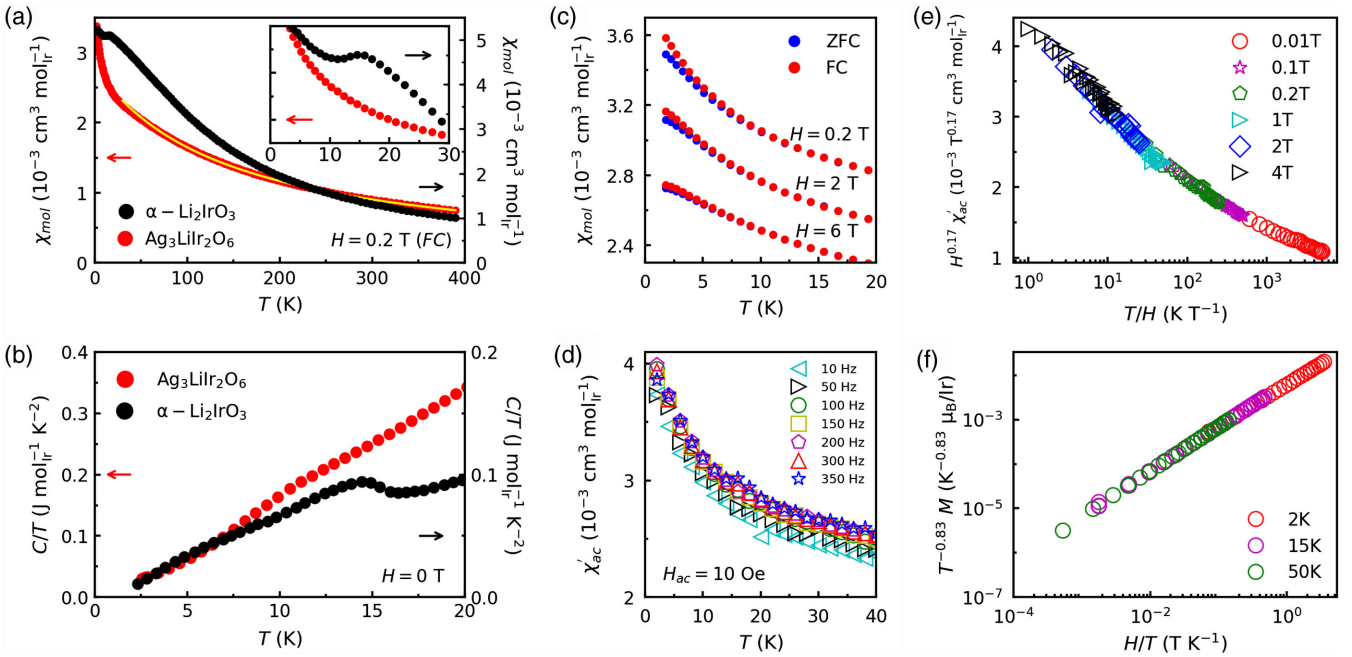

FIG. 2. (a) dc magnetic susceptibility as a function of temperature in $Ag_3LiIr_2O_6$ (red) and α-Li_2IrO_3 (black) with a magnified view below 30 K in the inset. The yellow line is a Curie-Weiss fit. (b) Heat capacity per mole Ir as a function of temperature in $Ag_3LiIr_2O_6$ (red) and α-Li_2IrO_3 (black data from Ref. [36]). (c) A small splitting in the dc susceptibility data under ZFC and FC conditions appears below 10 K. It disappears at higher fields. The curves are slightly shifted for visibility. (d) The real part of the ac susceptibility χ'_{ac} as a function of temperature. (e) Data collapse for $H^{\alpha}\chi'_{ac}$ as a function of T/H on a semilog scale with $\alpha = 0.17$. (f) Data collapse for $T^{\alpha-1}M$ as a function of H/T on a log-log scale.

and α-Li_2IrO_3. However, their magnetic behavior is different as discussed next.

Magnetism.—Figure 2(a) shows that the peak at $T_N = 15$ K in the magnetic susceptibility of α-Li_2IrO_3 due to the AFM ordering is absent in $Ag_3LiIr_2O_6$. Similarly, Fig. 2(b) confirms the absence of a peak in the heat capacity of $Ag_3LiIr_2O_6$ unlike the peak at 15 K in α-Li_2IrO_3. However, a slight change of slope is discernible in $Ag_3LiIr_2O_6$ at $T_L = 13$ K. These observations suggest that the second-order AFM transition in α-Li_2IrO_3 is replaced by a crossover in $Ag_3LiIr_2O_6$. The yellow line in Fig. 2(a) is a fit to the expression $\chi = \chi_0 + [C/(T - \Theta_{CW})]$ which yields a Curie-Weiss temperature $\Theta_{CW} = -142$ K and a magnetic moment $\mu = 1.79\ \mu_B$ comparable to the reported values in α-Li_2IrO_3 (−105 K, 1.83 μ_B) [10,36]. This is consistent with the similar bond angles in Table I and confirms a comparable strength of the Heisenberg exchange interaction in both compounds.

A small splitting between the zero-field-cooled (ZFC) and field-cooled (FC) curves is observed below 10 K [Fig. 2(c)] that suggests a trace of spin glasslike freezing. As seen in Figs. 2(c) and 2(d), this splitting is only 3% of the total magnetization, vanishes at higher fields, and does not produce a peak in the ac susceptibility. Thus, it originates from a minority of frozen spins (quenched disorder) while the majority of the system remains in a paramagnetic QSL state. A universal behavior among QSL materials with quenched disorder is a data collapse as reported in $H_3LiIr_2O_6$, $LiZn_2Mo_3O_8$, $ZnCu_3(OH)_6Cl_2$, and Cu_2IrO_3 [21,23,37,38]. The data collapse results from a subset of random singlets induced by a small amount of disorder within either a spin-liquid or a valence-bond-solid (VBS) ground state [23]. Figure 2(e) presents a data collapse of $H^{0.17}\chi_{ac}$ as a function of T/H over three decades of the scaling parameter. Similarly, Fig. 2(f) shows a scaling of $T^{-0.83}M$ as a function of H/T. These scaling analyses confirm the presence of random singlets in $Ag_3LiIr_2O_6$ but cannot distinguish between a spin-liquid or a VBS ground state.

Heat capacity.—As mentioned in the introduction, the MC simulations suggest that a Kitaev magnet releases the spin entropy in two successive crossovers at a higher (T_H) and a lower (T_L) temperature [8]. In three dimensions, for example, in a hyperhoneycomb lattice, these crossovers turn into phase transitions [39,40]. Figure 3(a) presents C/T (per mole Ir or Sn) as a function of temperature in $Ag_3LiIr_2O_6$ and $Ag_3LiSn_2O_6$, where the stannate is used to subtract the phonon background from the iridate. The resulting magnetic heat capacity C_m is plotted as a function of T in Fig. 3(b) and used to calculate the magnetic entropy via $S_m = \int (C_m/T)dT$ that reveals a two step structure. The first step is broad and corresponds to the broad hump at $T_H \approx 75$ K in C_m. The second step is better resolved and corresponds to the peak at $T_L = 13$ K in C_m. Neither of these features are sharp; i.e., they are more likely to be crossovers instead of second-order AFM transitions.

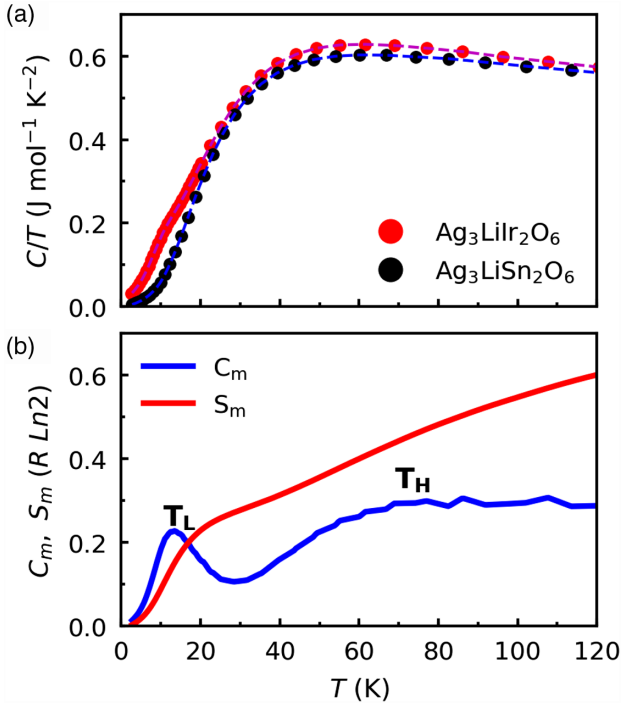

FIG. 3. (a) Heat capacity (C/T per mole Ir or Sn) plotted as a function of temperature in $Ag_3LiIr_2O_6$ and its lattice model $Ag_3LiSn_2O_6$. (b) Magnetic heat capacity (C_m) and entropy (S_m) plotted in units of $R\ln(2)$ as a function of temperature. Two broad features are revealed at $T_H \approx 75$ and $T_L = 13$ K.

This behavior is qualitatively consistent with MC simulations [8,9]; however, two deviations from the theory must be pointed out. (a) According to theory, the entropy release at each step must be $\frac{1}{2}R\ln(2)$, but we observe 60% of this value. A similar observation is reported in the parent compound, α-Li_2IrO_3, and the quantitative disagreement is attributed to the phonon background subtraction [10]. It is possible that $Ag_3LiSn_2O_6$ is not a perfect lattice model. (b) Ideally, the ratio of T_L/T_H should be less than 0.03 for a Kitaev spin liquid [8,9], but $T_L/T_H = 0.17$ in $Ag_3LiIr_2O_6$, similar to both α-Li_2IrO_3 and Na_2IrO_3 [10]. Note that the MC simulations were performed on an ideal system with purely Kitaev interactions. Because the real candidate materials have additional non-Kitaev interactions [Eq. (1)], it is expected to find mild deviations from the ideal theoretical results.

Discussion.—At this point, it is instructive to compare the structural and magnetic parameters between $Ag_3LiIr_2O_6$ and α-Li_2IrO_3 (Table II). Because of a comparable bond angle ϕ, the cancellation of Heisenberg interactions across the opposite Ir-O-Ir bonds in Fig. 1(b) must be comparable in both compounds. A comparison of Θ_{CW} and Ir-Ir distance suggests that the exchange coupling strength is also comparable in both compounds. The main structural difference between the two materials is a 30% larger interlayer separation in $Ag_3LiIr_2O_6$. At first glance, an increased interlayer separation may suggest increased magnetic fluctuations, hence a weaker AFM order. However, the exchange interactions in iridate materials are highly anisotropic [41] and such an argument does not justify the complete suppression of the AFM order in $Ag_3LiIr_2O_6$.

TABLE II. Comparing the experimental values of the average Ir-O-Ir bond angle (ϕ), Curie-Weiss temperature (Θ_{CW}), interlayer separation (d), and Ir–Ir distance between $Ag_3LiIr_2O_6$ and α-Li_2IrO_3. The c-axis parameter and the monoclinic angle β for α-Li_2IrO_3 are from Ref. [26] and Θ_{CW} is from Ref. [10].

	$Ag_3LiIr_2O_6$	α-Li_2IrO_3
$\bar{\phi}$	96.7°	95.0°
Θ_{CW}	−142 K	−105 K
$d = c\sin(\beta)$	6.24 Å	4.82 Å
Ir-Ir	3.04 Å	2.98 Å

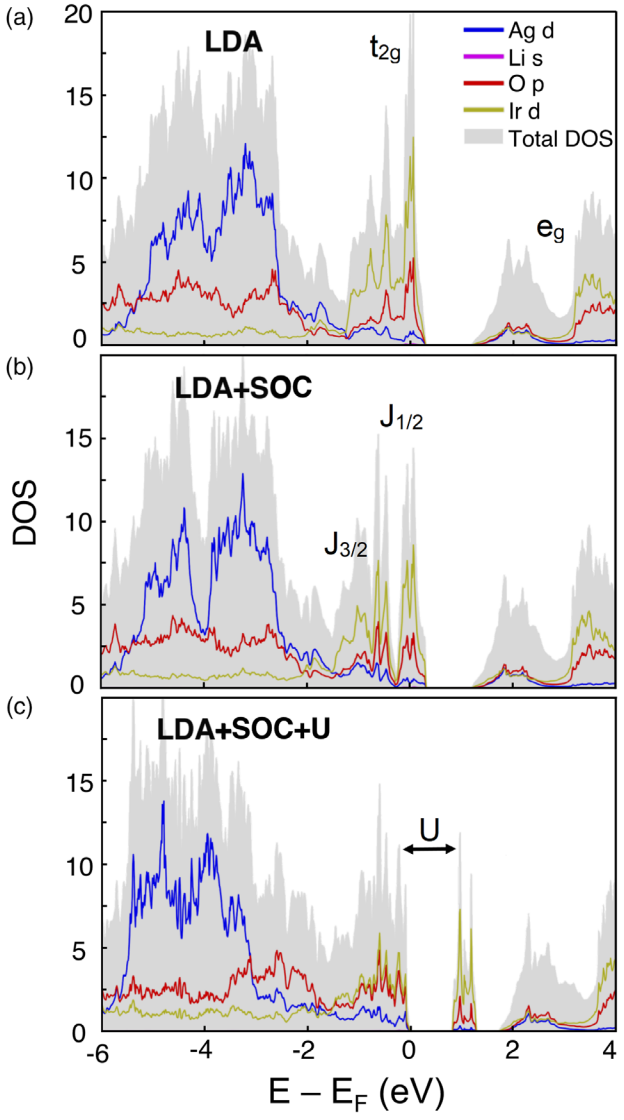

FIG. 4. Density of states calculated at three levels of DFT with (a) local density approximation (LDA), (b) LDA + SOC, and (c) LDA + SOC + U, where U is the exchange potential.

A more plausible explanation for the lack of AFM order comes from the density of states (DOS) calculations presented in Fig. 4 where a finite weight of silver $4d$ orbitals is observed at the Fermi level E_F. We present three levels of the DFT calculations following the prior work on α-Li_2IrO_3 [42]. First, a plain local density approximation (LDA) is presented in Fig. 4(a) to show the t_{2g} states just below E_F and e_g states above E_F. Notice that the majority of Ag electrons (blue line) are between 2 and 4 eV below E_F; however, a small but finite contribution from silver d orbitals is observed near E_F. Second, by adding the spin-orbit coupling (LDA + SOC) in Fig. 4(b), the t_{2g} levels are split into lower $J_{\text{eff}} = 3/2$ and an upper $J_{\text{eff}} = 1/2$ states. Third, by adding an exchange potential (LDA + SOC + U) in Fig. 4(c), a gap is opened within the $J_{\text{eff}} = 1/2$ states to separate the upper and lower Hubbard bands [17]. These results are identical to α-Li_2IrO_3 and consistent with the localized effective spin-1/2 Kitaev model [42]. The new finding is the finite weight of silver $4d$ orbitals at E_F which remains unchanged between the LDA and LDA + SOC + U calculations, and suggests a d-p orbital mixing between the Ag and O atoms. Whereas the lithium $2s$ electrons in α-Li_2IrO_3 are transferred to oxygen $2p$ orbitals in an ionic bond, the silver $4d$ electrons in $Ag_3LiIr_2O_6$ are more extended and bonded to the oxygen $2p$ orbitals with a more covalent character. As a result of such d-p mixing, the SOC is effectively increased on the Ir-O-Ir exchange path within the honeycomb layers of $Ag_3LiIr_2O_6$ which enhances the Kitaev coupling. We emphasize that despite comparable Ir-O-Ir bond angles between α-Li_2IrO_3 and $Ag_3LiIr_2O_6$ within the honeycomb layers (Table I), the latter compound is closer to the Kitaev limit because of a stronger SOC mediated via the O-Ag-O bonds between the layers. Thus, our work presents a new approach to optimizing the Kitaev magnets by tuning the interlayer instead of intralayer chemical bonds.

We thank I. Kimchi, Y. Ran, N. Perkins, and D. Haskel for fruitful discussions. The work at Boston College was supported by the National Science Foundation under Grant No. DMR–1708929. Work at Los Alamos was conducted under the auspices of the U.S. Department of Energy, Office of Basic Energy Sciences, Division of Materials Sciences and Engineering. O. I. L acknowledges financial support from the "Agence Nationale de la Recherche" in the framework of the "Investissements d'avenir" program with the reference "ANR–11–EQPX–0020" for EELS data obtained using GIF Quantum. This work was granted access to the HPC resources of [TGCC/CINES/IDRIS] under allocation 2017-A0010907682 made by GENCI.

*fazel.tafti@bc.edu

[1] J. Knolle and R. Moessner, Annu. Rev. Condens. Matter Phys. **10**, 451 (2019).
[2] H. Takagi, T. Takayama, G. Jackeli, G. Khaliullin, and S. E. Nagler, Nat. Rev. Phys. **1**, 264 (2019).
[3] L. Savary and L. Balents, Rep. Prog. Phys. **80**, 016502 (2017).
[4] S. M. Winter, Y. Li, H. O. Jeschke, and R. Valentì, Phys. Rev. B **93**, 214431 (2016).
[5] A. Kitaev, Ann. Phys. **321**, 2 (2006).
[6] G. Jackeli and G. Khaliullin, Phys. Rev. Lett. **102**, 017205 (2009).
[7] M. Hermanns, I. Kimchi, and J. Knolle, Annu. Rev. Condens. Matter Phys. **9**, 17 (2018).
[8] J. Nasu, M. Udagawa, and Y. Motome, Phys. Rev. B **92**, 115122 (2015).
[9] Y. Yamaji, T. Suzuki, T. Yamada, S.-i. Suga, N. Kawashima, and M. Imada, Phys. Rev. B **93**, 174425 (2016).
[10] K. Mehlawat, A. Thamizhavel, and Y. Singh, Phys. Rev. B **95**, 144406 (2017).
[11] S. K. Choi, R. Coldea, A. N. Kolmogorov, T. Lancaster, I. I. Mazin, S. J. Blundell, P. G. Radaelli, Y. Singh, P. Gegenwart, K. R. Choi, S.-W. Cheong, P. J. Baker, C. Stock, and J. Taylor, Phys. Rev. Lett. **108**, 127204 (2012).
[12] S. C. Williams, R. D. Johnson, F. Freund, S. Choi, A. Jesche, I. Kimchi, S. Manni, A. Bombardi, P. Manuel, P. Gegenwart, and R. Coldea, Phys. Rev. B **93**, 195158 (2016).
[13] S. Choi, S. Manni, J. Singleton, C. V. Topping, T. Lancaster, S. J. Blundell, D. T. Adroja, V. Zapf, P. Gegenwart, and R. Coldea, Phys. Rev. B **99**, 054426 (2019).
[14] J. G. Rau, E. K.-H. Lee, and H.-Y. Kee, Phys. Rev. Lett. **112**, 077204 (2014).
[15] S. D. Das, S. Kundu, Z. Zhu, E. Mun, R. D. McDonald, G. Li, L. Balicas, A. McCollam, G. Cao, J. G. Rau, H.-Y. Kee, V. Tripathi, and S. E. Sebastian, Phys. Rev. B **99**, 081101 (2019).
[16] S. Hwan Chun, J.-W. Kim, J. Kim, H. Zheng, C. C. Stoumpos, C. D. Malliakas, J. F. Mitchell, K. Mehlawat, Y. Singh, Y. Choi, T. Gog, A. Al-Zein, M. M. Sala, M. Krisch, J. Chaloupka, G. Jackeli, G. Khaliullin, and B. J. Kim, Nat. Phys. **11**, 462 (2015).
[17] See Supplemental Material at http://link.aps.org/supplemental/10.1103/PhysRevLett.123.237203 for the details.
[18] K. W. Plumb, J. P. Clancy, L. J. Sandilands, V. V. Shankar, Y. F. Hu, K. S. Burch, H.-Y. Kee, and Y.-J. Kim, Phys. Rev. B **90**, 041112(R) (2014).
[19] H. B. Cao, A. Banerjee, J.-Q. Yan, C. A. Bridges, M. D. Lumsden, D. G. Mandrus, D. A. Tennant, B. C. Chakoumakos, and S. E. Nagler, Phys. Rev. B **93**, 134423 (2016).
[20] S. Bette, T. Takayama, K. Kitagawa, R. Takano, H. Takagi, and R. E. Dinnebier, Dalton Trans. **46**, 15216 (2017).
[21] K. Kitagawa, T. Takayama, Y. Matsumoto, A. Kato, R. Takano, Y. Kishimoto, S. Bette, R. Dinnebier, G. Jackeli, and H. Takagi, Nature (London) **554**, 341 (2018).
[22] J. Knolle, R. Moessner, and N. B. Perkins, Phys. Rev. Lett. **122**, 047202 (2019).
[23] I. Kimchi, J. P. Sheckelton, T. M. McQueen, and P. A. Lee, Nat. Commun. **9**, 4367 (2018).
[24] J. Rodríguez-Carvajal, Physica (Amsterdam) **192B**, 55 (1993).

[25] K. Momma and F. Izumi, J. Appl. Crystallogr. **44**, 1272 (2011).
[26] M. J. OMalley, H. Verweij, and P. M. Woodward, J. Solid State Chem. **181**, 1803 (2008).
[27] V. Todorova, A. Leineweber, L. Kienle, V. Duppel, and M. Jansen, J. Solid State Chem. **184**, 1112 (2011).
[28] S. Bette, T. Takayama, V. Duppel, A. Poulain, H. Takagi, and R. E. Dinnebier, Dalton Trans. **48**, 9250 (2019).
[29] J. H. Roudebush, N. H. Andersen, R. Ramlau, V. O. Garlea, R. Toft-Petersen, P. Norby, R. Schneider, J. N. Hay, and R. J. Cava, Inorg. Chem. **52**, 6083 (2013).
[30] M. Abramchuk, O. I. Lebedev, O. Hellman, F. Bahrami, N. E. Mordvinova, J. W. Krizan, K. R. Metz, D. Broido, and F. Tafti, Inorg. Chem. **57**, 12709 (2018).
[31] M. Abramchuk, C. Ozsoy-Keskinbora, J. W. Krizan, K. R. Metz, D. C. Bell, and F. Tafti, J. Am. Chem. Soc. **139**, 15371 (2017).
[32] D. Balzar, J. Res. Natl. Inst. Stand. Technol. **98**, 321 (1993).
[33] G. Kresse and J. Furthmüller, Comput. Mater. Sci. **6**, 15 (1996).
[34] D. M. Ceperley and B. J. Alder, Phys. Rev. Lett. **45**, 566 (1980).
[35] A. I. Liechtenstein, V. I. Anisimov, and J. Zaanen, Phys. Rev. B **52**, R5467 (1995).
[36] Y. Singh, S. Manni, J. Reuther, T. Berlijn, R. Thomale, W. Ku, S. Trebst, and P. Gegenwart, Phys. Rev. Lett. **108**, 127203 (2012).
[37] E. M. Kenney, C. U. Segre, W. Lafargue-Dit-Hauret, O. I. Lebedev, M. Abramchuk, A. Berlie, S. P. Cottrell, G. Simutis, F. Bahrami, N. E. Mordvinova, G. Fabbris, J. L. McChesney, D. Haskel, X. Rocquefelte, M. J. Graf, and F. Tafti, Phys. Rev. B **100**, 094418 (2019).
[38] Y. S. Choi, C. H. Lee, S. Lee, S. Yoon, W.-J. Lee, J. Park, A. Ali, Y. Singh, J.-C. Orain, G. Kim, J.-S. Rhyee, W.-T. Chen, F. Chou, and K.-Y. Choi, Phys. Rev. Lett. **122**, 167202 (2019).
[39] I. Kimchi, J. G. Analytis, and A. Vishwanath, Phys. Rev. B **90**, 205126 (2014).
[40] J. Nasu, T. Kaji, K. Matsuura, M. Udagawa, and Y. Motome, Phys. Rev. B **89**, 115125 (2014).
[41] Y. Sizyuk, C. Price, P. Wölfle, and N. B. Perkins, Phys. Rev. B **90**, 155126 (2014).
[42] Y. Li, K. Foyevtsova, H. O. Jeschke, and R. Valentí, Phys. Rev. B **91**, 161101(R) (2015).